HHS Public Access

Author manuscript

Cell Rep Phys Sci. Author manuscript; available in PMC 2024 April 11.

Published in final edited form as:

Cell Rep Phys Sci. 2024 March 20; 5(3): . doi:10.1016/j.xcrp.2024.101869.

Polyproline peptide targets *Klebsiella pneumoniae* polysaccharides to collapse biofilms

Laura De los Santos[1], **Robert L. Beckman IV**[1], **Christina DeBarro**[1], **James E. Keener**[2], **Marcelo D.T. Torres**[3,4,5,6], **Cesar de la Fuente-Nunez**[3,4,5,6], **Jennifer S. Brodbelt**[2], **Renee M. Fleeman**[1,7,8,*]

[1]Division of Immunity and Pathogenesis, Burnett School of Biomedical Sciences, College of Medicine, University of Central Florida, Orlando, FL 32827, USA

[2]Department of Chemistry, The University of Texas at Austin, Austin, TX 78712, USA

[3]Machine Biology Group, Departments of Psychiatry and Microbiology, Institute for Biomedical Informatics, Institute for Translational Medicine and Therapeutics, Perelman School of Medicine, University of Pennsylvania, Philadelphia, PA 19104, USA

[4]Departments of Bioengineering and Chemical and Biomolecular Engineering, School of Engineering and Applied Science, University of Pennsylvania, Philadelphia, PA 19104, USA

[5]Department of Chemistry, School of Arts and Sciences, University of Pennsylvania, Philadelphia, PA, USA

[6]Penn Institute for Computational Science, University of Pennsylvania, Philadelphia, PA 19104, USA

[7]X (formerly Twitter): @FleemanLab

[8]Lead contact

SUMMARY

Hypervirulent *Klebsiella pneumoniae* is known for its increased extracellular polysaccharide production. Biofilm matrices of hypervirulent *K. pneumoniae* have increased polysaccharide abundance and are uniquely susceptible to disruption by peptide bactenecin 7 (bac7 (1–35)). Here, using confocal microscopy, we show that polysaccharides within the biofilm matrix collapse following bac7 (1–35) treatment. This collapse led to the release of cells from the biofilm, which were then killed by the peptide. Characterization of truncated peptide analogs revealed that their interactions with polysaccharide were responsible for the biofilm matrix changes that accompany

*Correspondence: renee.fleeman@ucf.edu.

AUTHOR CONTRIBUTIONS

R.M.F. conceived the idea and designed the experimentation. The biofilm experiments were performed by R.M.F., L.D.l.S., R.L.B., and C.D. The UVPD native mass spectrometry work was performed and the data were processed by J.E.K. and J.S.B. C.D. produced the AlphaFold images and BioRender vectors. M.D.T.T. and C.d.l.F.-N. performed the HEK293T toxicity, blood lysis, and murine skin abscess infection, and collected and graphed the results. R.M.F. wrote the text and discussed the results with L.D.l.S. L.D.l.S., R.L.B., J.E.K., J.S.B., C.d.l.F.-N., and M.D.T.T. participated in manuscript editing for the final manuscript.

SUPPLEMENTAL INFORMATION

Supplemental information can be found online at https://doi.org/10.1016/j.xcrp.2024.101869.

bac7 (1–35) treatment. Ultraviolet photodissociation mass spectrometry with the parental peptide or a truncated analog bac7 (10–35) reveal the important regions for bac7 (1–35) complexing with polysaccharides. Finally, we tested bac7 (1–35) using a murine skin abscess model and observed a significant decrease in the bacterial burden. These findings unveil the potential of bac7 (1–35) polysaccharide interactions to collapse *K. pneumoniae* biofilms.

Graphical Abstract

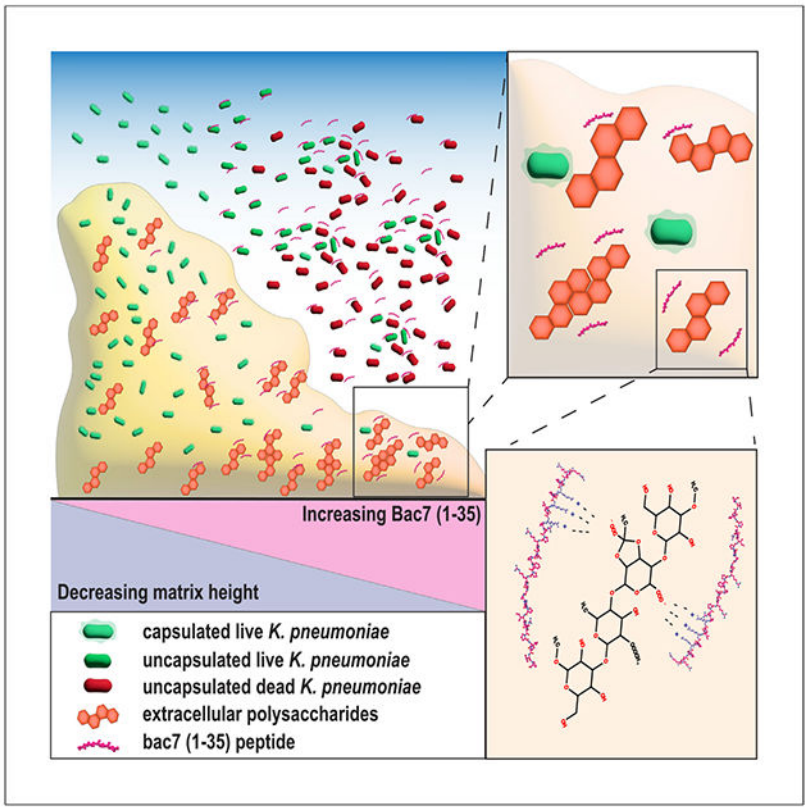

De los Santos et al. use confocal microscopy to study biofilm matrix collapse by the defense peptide bac7 (1–35). The polysaccharide interactions of bac7 (1–35) cause the release of the biofilm cells and collapse of hypervirulent *Klebsiella pneumoniae* biofilms.

INTRODUCTION

Klebsiella pneumoniae infections have been increasingly problematic in recent years.[1–9] This is in part due to an increase in drug resistance acquisition over the last decades, leading to infections that are resistant to almost all available clinical antibiotics.[10–13] In addition to drug resistance acquisition, the emergence of hypervirulent *K. pneumoniae* isolates has enabled the spread of infections within healthy individuals.[14,15] A defining characteristic of hypervirulent *K. pneumoniae* is the hypermucoviscous phenotype provided by an increase in capsular polysaccharides.[16–18] In addition to capsule, extracellular polysaccharides are also found within the biofilm matrix[19] and play a major role in maintaining the integrity of the

biofilm and preventing the collapse of the matrix.[20–22] Biofilms formed by *K. pneumoniae* increase their resistance to the host immune system and antibiotic therapy.[23,24]

Antimicrobial peptides have shown promise in recent years as a topical therapy for the treatment of multi-drug resistant infections.[25–31] We have shown that PepW, a synthetic α-helical peptide, can disrupt the capsule of hypervirulent *K. pneumoniae*.[32] We determined it was the loss of peptide structure when interacting with capsular polysaccharides that caused aggregate formation and consequently *K. pneumoniae* capsule disruption. Further investigation revealed that polyproline host defense peptide bactenecin 7 (bac7 (1–35)) formed robust polysaccharide aggregates and disrupted the biofilm of hypervirulent *K. pneumoniae*.[33] These results were intriguing because bac7 (1–35) has been described as attaining its bactericidal activity from protein synthesis inhibition instead of membrane disruption that is characteristic of most cationic antimicrobial peptides.[34] Moreover, bac7 (1–35) has been shown to have multiple mechanisms of action that varies depending on the bacterial species being tested.[35] Considering the multiple mechanisms used by bac7 (1–35), we hypothesized that this peptide may interact with *K. pneumoniae* capsular polysaccharides as well as biofilm-associated polysaccharides.

Here, we combine phenotypic biofilm analysis with confocal microscopy to reveal that the loss of viability following treatment with bac7 (1–35) is due to the collapse of the polysaccharide matrix. Our analysis of truncated bac7 (1–35) analogs with different antimicrobial activities revealed that polysaccharide interactions with bac7 (1–35) play an important role in the mechanism of biofilm collapse. Characterization of peptide·polysaccharide complexes by ultraviolet photodissociation (UVPD) mass spectrometry identified the interaction region between the peptide and polysaccharide. Finally, we show that treatment with bac7 (1–35) significantly decreased the bacterial burden of hypervirulent *K. pneumoniae* NTUH K2044 using a murine skin abscess model. These findings highlight the potential of polyproline peptides interactions with extracellular polysaccharides as a mechanism to disrupt *K. pneumoniae* biofilms.

RESULTS

Bac7 (1–35) treatment induces matrix polysaccharide collapse and release of biofilm-associated cells

We previously found that bac7 (1–35) was able to disrupt the biofilm of hypervirulent isolates more effectively than those of classical *K. pneumoniae*.[33] This finding led to our hypothesis that the increased thickness observed with hypervirulent biofilms was due to an excess of polysaccharides making these biofilms more susceptible to disruption by polysaccharide-interacting peptides. Therefore, to confirm this hypothesis, we tested whether bac7 (1–35) was able to target biofilm matrix polysaccharides, ultimately eradicating pre-formed biofilms of hypervirulent *K. pneumoniae*. To determine the change in matrix polysaccharides, we used *K. pneumoniae* NTUH K2044 carrying pMF230 constitutively expressing GFP to grow the biofilms and stained the biofilms with Texas red-conjugated concanavalin A for visualization of the matrix-associated polysaccharides.[36] Concanavalin A Texas red conjugate binding to α-mannopyranosyl and α-glucopyranosyl polysaccharides has been described previously[37] and the specificity to matrix-associated

polysaccharides was shown by the absence of biofilm staining with a bacterial mutant lacking exopolysaccharide production.[38]

Using a multi-level approach (Figure 1), our analysis included bacterial recovery to assess the dose-dependent biofilm eradication abilities of bac7 (1–35) within the petri dishes that were then used to visualize the biofilms. This allowed for direct comparison of the cellular viability to our confocal imaging. We found that treatment of pre-formed biofilms of *K. pneumoniae* NTUH K2044 with bac7 (1–35) at concentrations above the minimal inhibitory concentration resulted in significant loss of the biofilm cell viability (Figure 2A). Specifically, treatment with 7.5 μmol L^{-1} of bac7 (1–35) had little effect on the viability of the cells within the biofilm. However, when the concentration of bac7 (1–35) was increased to 15 and 30 μmol L^{-1} there was a 2-log and a 5-log decrease in viability, respectively. This dose-dependent eradication of the biofilm could be a result of the release of viable dispersed cells to spread the infection. Therefore, we also assessed the viability of the dispersed cell population of these biofilms and found there was significant death of the dispersed cells with all concentrations of peptide tested (Figure S1A). In addition, we performed a mucoviscosity assessment[33] to analyze the hypermucoviscous phenotype of the dispersed cell population following treatment of the biofilms with 7.5, 15, and 30 μmol L^{-1} of bac7 (1–35). Our analysis revealed a significant change in the hypermucoviscous phenotype of *K. pneumoniae* NTUH K2044 dispersed cells following bac 7 (1–35) treatment at all concentrations tested (Figure S2).

We then treated pre-formed biofilms in glass-bottom petri dishes to allow for confocal microscopy visualization. With no treatment, the *K. pneumoniae* NTUH K2044 biofilm had a height of ~20 μm with cells residing on multiple levels of the biofilm (Figure 2B). When treated with 7.5 μmol L^{-1}, in agreement with our biofilm viability assessment bac7 (1–35) had a minor effect on the polysaccharide matrix or the cells embedded within the matrix (Figure 2C). However, at 15 μmol L^{-1} the upper layers of the biofilm are absent, the biofilm collapses, and only the polysaccharides at the base of the biofilm remain (Figure 2D). Increasing the concentration of bac7 (1–35) to 30 μmol L^{-1} resulted in similar collapse (data not shown). We then wanted to build a kinetic picture of the *K. pneumoniae* biofilm response to 15 μmol L^{-1} bac7 (1–35). When assessing the viability of both the biofilm and dispersed cells over 4 h, we found significant decrease in viability of the biofilm after 4 h (Figure 2E) and viability of the dispersed cells decreased after 2 h (Figure S1B). When imaging the biofilms after 1 h of treatment, we can observe the cells within the upper layer of the biofilm begin to release (Figure 2F). Following 2 h incubation, we observed the complete loss of the cells residing in the upper layer of the biofilm (Figure 2G). Finally, after 4-h incubation, we observed the collapsed biofilm similar to that observed after 24 h (Figure 2H). Overall, our multi-level analyses show that bac7 (1–35) treatment of *K. pneumoniae* NTUH K2044 biofilms results in the collapse of the biofilm matrix and death of the released dispersed cells.

Biofilm matrix modulation by bac7 (1–35) analogs is not correlated with antimicrobial activity but extracellular polysaccharide interactions

To understand the physiochemical properties of bac7 (1–35) that are necessary to cause collapse of the biofilm of *K. pneumoniae* NTUH K2044, we tested previously studied bac7 analogs that have been shown to vary in their antimicrobial activity.[39,40] These include N-terminal and C-terminal truncated analogs and one analog that contains amino acid residues 24–59 from the full-length peptide bactenecin 7.[39] Before further assessment, we verified the bac7 (1–35) analogs' antimicrobial activity toward *K. pneumoniae* NTUH K2044 and found that, as shown before,[39,40] the truncated analogs have variable activities (Table 1). We have previously shown that bac7 (1–35) can aggregate with extracellular polysaccharides, an attribute important for capsule disruption of hypermucoviscous *K. pneumoniae*.[33] Our analysis comparing the *K. pneumoniae* NTUH K2044 biofilm polysaccharides and the cell attached polysaccharides revealed the similarity between these two samples, which is in line with previous *K. pneumoniae* biofilm analysis findings (Figures S3A–S3G).[41] Therefore, we hypothesized that the extracellular polysaccharide aggregation potential of our analogs could be used to delineate the properties of bac7 (1–35) that are important for the collapse of the biofilm matrix. Each analog was mixed at a concentration of 100 μmol L^{-1} with purified extracellular polysaccharides from *K. pneumoniae* NTUH K2044 to determine their aggregation abilities. We found that the aggregation potential of the analogs did not follow antimicrobial activity as we described in our previous work with a synthetic α-helical peptide.[32] Instead, aggregation correlated with net positive charge as bac7 (5–35), bac7 (1–24), bac7 (1–16), and bac7 (24–59), with charges of +8, +9, +8, and +8, respectively, had the highest aggregation potential (Figures 3A and S3H). From this analysis we calculated the relative extracellular polysaccharide aggregation (EPS^{RA}) abilities of the analogs compared with the parental bac7 (1–35) peptide (Table 1). Interestingly, bac7 (24–59), with a charge of +8 had no antimicrobial activity but a relative extracellular aggregation value of 0.32. To determine the effect of extracellular polysaccharides on the peptide we assessed the secondary structure of all peptides using far UV circular dichroism (260–190 nm) (Figure S4). We observed that the truncated analogs had a decrease in amplitude at their spectral minima (~200 nm), a known consequence of shortened peptide length.[42] With the addition of extracellular polysaccharides to analogs with aggregative properties, we observed a greater decrease in amplitude of the mean residue ellipticity at the spectral minima (<200 nm) (Figures S4A, S4B, S4G, and S4K) than with peptides that did not form aggregates (Figures S4C–S4F and S4H–S4J). In addition to decreasing the amplitude of the peptide mean residue ellipticity, the presence of polysaccharide also caused a shift in the wavelength (200–212 nm) for the spectral minima for the parental bac7 (1–35), bac7 (5–35), bac7 (5–24), bac7 (9–24), and bac7 (24–59) (Figures S4A, S4B, S4E, S4F, and S4K). Our aggregation and far UV circular dichroism results reveal that the loss of structure is associated with aggregation as we described in our previous work.[32]

We then used the same conditions as Figure 2 to compare the effects of treatment with each of the analogs on the polysaccharide matrix. We tested the analogs at a concentration of 15 μmol L^{-1}, which was the lowest concentration where bac7 (1–35) causes collapse of the polysaccharide matrix. Our results show that most analogs did not influence the height of the matrix as strongly as the parental peptide (Figure S5). However, biofilms

treated with analogs bac7 (24–59), bac7 (5–35), and bac7 (1–16) (Figures S5C, S5D, and S5I) displayed a drop in overall height (30 μm) and moderate change in the polysaccharide matrix. To expand on this, we tested increased concentrations of the inactive peptides bac7 (24–59) and bac7 (10–35), which displayed moderate polysaccharide interactions. We found treatment with bac7 (24–59) but not bac7 (10–35) at 60 μmol L^{-1} resulted in the polysaccharide matrix loss from the upper layers of the biofilm (Figures 3B and 3C). As expected, the biofilm and dispersed CFU mL^{-1} did not significantly change with treatment of either bac7 (24–59) or bac7 (10–35), although there was a slight decrease in biofilm and corresponding increase in the dispersed population with bac7 (24–59) treatment (Figure S1C and S1D). Therefore, we conclude that the full-length peptide is needed for the greatest matrix collapse, but peptides with little antimicrobial activity toward *K. pneumoniae* NTUH K2044 can induce polysaccharide matrix changes. Collectively, our analysis of the bac7 (1–35) analogs revealed that charge rather than antimicrobial activity is important for biofilm polysaccharide interactions.

UVPD native mass spectrometry reveals that interactions with stachyose drive the loss of peptide structure

We have previously reported on polysaccharide interactions with synthetic AMPs.[32] This work revealed distinct differences in amino acid binding to polysaccharides between a peptide with aggregative potential with *K. pneumoniae* capsular polysaccharides and an inactive peptide with no aggregative potential. Therefore, we wanted to characterize the differences in the non-covalent interactions of polysaccharide with the parental bac7 (1–35) and its truncated analog bac7 (10–35) that displayed limited aggregation with polysaccharides and caused no biofilm collapse. To accomplish this goal, we used native mass spectrometry[43–47] coupled with UVPD.[48–54] Native mass spectrometry allows transfer of non-covalent peptide · polysaccharide complexes to the gas phase, and UVPD is used to activate the complexes and produce diagnostic fragment ions in a way that is sensitive to both primary and secondary structure. UVPD of the peptide · polysaccharide complexes produces apo fragment ions (conventional sequence-type ions from the peptide) as well as holo fragment ions containing a portion of the peptide plus the bound polysaccharide.[50] Analyzing the holo-ions and ligand-free apo-ions allows identification of the key amino acids that may interact with polysaccharides and facilitates the assessment of the structural changes that accompany the formation or disruption of non-covalent interactions.[47–54] In essence, interaction of the polysaccharide with the peptide results in non-covalent interactions that may either stabilize regions of the peptide and suppress release of fragment ions upon UVPD or enhance the production of other fragment ions not favored for the apo peptide. The polysaccharide binding region of the peptide is determined by the overlap of N and C terminus holo-ions that originate from backbone cleavages of the peptide.

The complex nature of bacterial extracellular polysaccharides results in extremely heterogeneous populations of polysaccharides that impede analysis of specific peptide · polysaccharide complexes by mass spectrometry. Therefore, as done with our previous work, we used the tetrasaccharide stachyose as a surrogate to analyze polysaccharide interactions with bac7 (1–35) and bac7 (10–35). The UVPD fragmentation patterns of bac7 (1–35) · stachyose (5+ charge state) and bac7 (10–35) · stachyose (4+ charge state) are shown as

peptide backbone cleavage graphs in Figures 4A and 4B (based on holo fragment ions). Figures S6A and S6B show the apo fragment ions for the peptide · stachyose complexes and Figures S6C and S6D for the apo peptides (only apo fragment ions). The patterns of fragment ions are mapped based on the backbone cleavage sites from which they originate. We examined the overlapping N- and C-terminal holo-ions for bac7 (1–35) · stachyose (Figure 4A) and bac7 (10–35) · stachyose (Figure 4B) to identify the regions of the peptides involved in interacting with the polysaccharide. Specifically, the interaction region was predicted by the overlap of both N- and C-terminal fragment ions that retain stachyose (holo-ions) and "bracket" the amino acid residues from Arg6 to Pro13 (Figure 4A). This region shifts to Leu9 and Pro12 (Figure 4B) for truncated bac7 (10–35), revealing a smaller interaction region for this analog.

Differential fragmentation graphs reveal the variations in fragmentation when comparing UVPD of bac7 (1–35) · stachyose (5+) relative to apo bac7 (1–35) (5+) (Figure 4C) and UVPD of bac7 (10–35) · stachyose (4+) relative to apo bac7 (10–35) (4+) (Figure 4D). Suppression of fragmentation of peptide · stachyose complexes relative to the apo peptides is shown as negative values, indicating structural stabilization (and decreased release of fragment ions). Conversely, positive values indicate an increase in fragmentation of the peptide · stachyose complexes relative to the apo peptides, corresponding to structural destabilization of peptides when bound to stachyose (i.e., enhanced fragmentation efficiency of the apo peptide relative to the holo peptide). The difference plots in Figures 4C and 4D reveal broad suppression of fragmentation of both the bac7 (1–35) · stachyose and bac7 (10–35) · stachyose complexes, indicating an overall increase in structural organization consistent with formation of stabilizing non-covalent interactions between the peptide and stachyose. For bac7 (1–35) · stachyose, we found one region of enhanced fragmentation (the N terminus region) relative to the apo peptide (Figure 4C). The increased fragmentation of the Arg2/Ile3 backbone position may be related to the fact that the polysaccharide engages in non-covalent interactions with a rather large section of the peptide spanning at least from residues Arg6 to Pro13, thus leaving the N-terminal region unencumbered, or owing to disruption of non-covalent interactions that otherwise stabilize the N-terminal region for the apo peptide. For the truncated bac7 (10–35) · stachyose complex, there were no areas of enhanced fragmentation compared with the apo peptide (Figure 4D). These findings reveal that the interaction region of bac7 (1–35) located between Arg6 and Pro13 contains arginine residues that may interact with polysaccharides causing stabilization of that region of the peptide, consequently destabilizing the Arg2/Ile3 region of the peptide and leading to aggregation in the presence of polysaccharide.

Bac7 (1–35) topical treatment reduces the bacterial burden in a murine skin abscess infection model

To show the potential of polyprolines as topical therapy for *K. pneumoniae* infected wounds, we used a murine skin abscess model to test the ability of bac7 (1–35) to decrease the bacterial burden.[55–59] This model can assess the ability of therapeutics to treat a type of infection where treatment is complicated by biofilm formation.[5,60,61] Initially, we assessed the toxicity profile of bac7 (1–35) to validate the absence of general mammalian cell cytotoxicity (Figure S7; Table S1). Our hemolysis results revealed bac7 (1–35) has a limited

ability to lyse red blood cells, as we did not see an increase in lysis as we increased the concentration of peptide (Figure S7). Furthermore, we found limited toxicity toward mammalian cell lines HepG2 and HEK293T with LD_{50} values of 15 and >30 μmol L^{-1}, respectively (Table S1). Although this level of hemolysis and cytotoxicity indicates systemic delivery would not be appropriate for this peptide, we were confident to move forward and test the ability of bac7 (1–35) to treat a wound infected with *K. pneumoniae* NTUH K2044.

We infected mice with 5×10^6 CFU mL^{-1} of *K. pneumoniae* NTUH K2044 onto a pre-formed linear skin abrasion and treated 1 h later with a single dose of 2 μmol L^{-1} bac7 (1–35) or 1 μmol L^{-1} polymyxin B (respective minimum inhibitory concentrations [MICs]). The mice were monitored for 4 days, and skin samples were assessed at day 2 and 4 for bacterial burden (Figure 5). After 2 days, there was a decrease in the bacterial burden with bac7 (1–35) treatment, although bac7 (1–35) did not decrease growth to the same extent as the positive control polymyxin B (Figure 5A). However, bacterial recovery after 4 days revealed a rebound in growth for the polymyxin B control group but not the bac7 (1–35) treated mice, which had similar bacterial recovery as on day 2 (Figure 5B). These results reveal that even a single dose at a very low concentration of bac7 (1–35) has potential as a topical treatment for wound infections caused by hypervirulent *K. pneumoniae*.

DISCUSSION

Extracellular polysaccharide production by *K. pneumoniae* allows evasion of the host immune system and resistance to therapeutic intervention.[21,62,63] We have previously shown that host defense peptide aggregation with extracellular polysaccharides allows for disruption of the capsule layer of *K. pneumoniae*.[32] Our investigation of this mechanism in host defense peptides revealed that bac7 (1–35) has the greatest antimicrobial activity, biofilm eradication, and polysaccharide aggregative properties.[33] We hypothesized that the biofilm disruption caused by bac7 (1–35) is dependent on the non-covalent interactions with polysaccharides.

The truncated analogs used in this study have been previously published to investigate the antimicrobial activity and ribosome binding capabilities.[35,40] Benincasa et al. found truncation from the N terminus decreases the antimicrobial activity more effectively than truncation from the C terminus.[39] In addition, the first 4 N-terminal amino acids were shown to be important for ribosome binding as bac7 (5–35) no longer efficiently binds to the exit tunnel.[40] We also found decreased antimicrobial activity with truncated analogs and found that truncation from the C terminus is better tolerated (Table 1). However, we found that truncation of more than four N-terminal amino acids is necessary to decrease the antimicrobial activity toward *K. pneumoniae* NTUH K2044. Bac7 (5–35) antimicrobial activity decreased from 0.5 to 4 μmol L^{-1}, while analog bac7 (10–35) had no antimicrobial activity. Furthermore, the polysaccharide interactions and biofilm modulation properties of the analogs do not correlate with the antimicrobial activity as bac7 (1–15) and bac7 (1–14) had minimal inhibitory concentrations of 2 μmol L^{-1} yet did not aggregate with extracellular polysaccharides or modulate the biofilm matrix (Figures 3A, S5J, and S5K). Our findings show that the spectrum of activities of polyproline peptides includes not only ribosome inhibition as previously discovered,[40] but also bacterial polysaccharide aggregation.

Polyproline peptides are helical peptides that attain their secondary structure by the steric hinderance created by prolines opposed to traditional α-helical peptides that use intramolecular hydrogen bonds between the heteroatoms along their backbone to drive their secondary structure.[64] This allows for polyproline peptides to interact with ligands more readily through non-covalent interactions.[65,66] The results from UVPD native mass spectrometry revealed the regions of the peptides involved in non-covalent interactions with stachyose, Arg6 to Pro13 for bac7 (1–35) and Leu9 to Pro12 for bac7 (10–35), both involve a proline residue (Figure 4). We propose a mechanism of bac7 (1–35) biofilm collapse where, in the presence of increasing bac7 (1–35) peptide, we observed matrix polysaccharide collapse in addition to capsular loss and death of the planktonic cells released from the biofilm. Based on our mass spectrometry findings and our identification of the importance of charge in biofilm collapse, we hypothesize that the arginine residues within the identified interaction region are complexing with polysaccharides. However, a more comprehensive analysis into the role of the proline residues of this peptide is necessary to fully understand bac7 (1–35) interactions with extracellular polysaccharides.

Considering the problematic treatment of wounds with biofilm infections and the propensity of hypervirulent *K. pneumoniae* to cause soft tissue infections,[67] we tested the ability of bac7 (1–35) to decrease the bacterial burden in a murine skin abscess infection model. Our results show that a single dose of bac7 (1–35) at low micromolar concentration can effectively limit the bacterial burden of a wound infection of hypervirulent *K. pneumoniae* NTUH K2044 4 days after infection (Figure 5). Interestingly, we saw an increase in the bacterial burden of polymyxin B-treated wounds from day 2 to day 4. This rebounding observed with the gold standard for topical treatment is very intriguing considering the increase in polymyxin B resistance in recent years.[5,68,69] Although our *in vivo* testing was limited in this study, it begins to reveal the potential of our peptide for wound treatment. Our future studies will focus on therapeutic optimization of bac7 (1–35) to increase the selectivity index and broaden the *in vivo* testing to include longer time intervals between infection and treatment.

Our work here highlights the potential of polyproline peptides as biofilm matrix disruptors through peptide · polysaccharide interactions. We revealed key proline amino acid parings that are important for the collapse of the biofilm matrix seen with bac7 (1–35). The decrease in bacterial burden seen in our skin abscess model is testament of the impact of polysaccharide interactions for wound treatment therapeutics. The interactions of polyproline peptides and extracellular polysaccharides warrants further investigation as to the potential impact on our ability to treat hypervirulent *K. pneumoniae* biofilm-related infections.

EXPERIMENTAL PROCEDURES

Resource availability

Lead contact—Requests for resources and reagents should be directed to the lead contact, Renee Fleeman (renee.fleeman@ucf.edu).

Material availability—The study did not generate new unique materials.

Data and code availability—All data reported in this paper will be shared by the lead contact upon reasonable request. This work did not generate any code.

Bacterial strains and growth conditions

Hypervirulent *K. pneumoniae* NTUH K2044 was used for all experiments in this study. For confocal microscopy we used a constitutive GFP expression plasmid pMF230 (deposited by Michael Franklin; Addgene plasmid no. 62546; http://n2t.net/addgene:62546; RRID: Addgene 62546) to allow visualization of the bacteria using fluorescence microscopy.[70] The strains were cultured using Luria-Bertani (LB) broth with supplementation of 300 μg mL^{-1} of carbenicillin when *K. pneumoniae* NTUH K2044 was grown harboring the plasmid for confocal microscopy.

Peptides

The bac7 (1–35) peptide was ordered from Novopro (https://www.novoprolabs.com/p/bac7-1-35–318782.html) and polymyxin B sulfate from TCI chemicals (https://www.tcichemicals.com). Novopro synthesized the bac7 analogs used in this study. All peptides were resuspended in ultra-purified water at 10 mg mL^{-1} and stored at −20°C. The net charge states of the peptides used in this study were determined using the peptide calculator at BACHEM (https://www.bachem.com/knowledge-center/peptide-calculator/). The structural images of bac7 (1–35) used for the figures were generated using AlphaFold's collaboration with google, found on https://colab.research.google.com/github/sokrypton/ColabFold/blob/main/AlphaFold2.ipynb#scrollTo=11l8k–10q0C.[71] We utilized the base parameters provided to us in their code to run the predictions. Structures were further analyzed using ChimeraX (https://www.rbvi.ucsf.edu/chimerax/).

Biofilm eradication

Overnight cultures of *K. pneumoniae* NTUH K2044 were diluted to an optical density at 600 nm (OD_{600}) of 0.5 (9.75×10^9 CFU mL^{-1}) in biofilm media (tryptic soy broth and 0.5% glucose). The biofilms were grown in 35 × 10 mm Petri dishes for 24 h at 37°C static before treatment with bac7 (1–35). The peptide was diluted into 1 mL of bovine serum albumin (BSA) buffer (0.2% BSA 0.01% acetic acid),[72] mixed with 7 mL Mueller Hinton Broth (MHB) to reach 30 μmol L^{-1}, serial diluted for the 15 and 7.5 μmol L^{-1} dilutions, and all dilutions were added to the biofilms. The no treatment control had 1 mL of BSA solution and 7 mL of MHB to account for the buffer addition. The biofilms were then incubated at 37°C static with the peptides for 24 h before dilution for enumeration. Colonies were counted to determine CFU mL^{-1} for the dispersed population and the biofilms that were resuspended in phosphate-buffered saline (PBS) after washing with PBS 3 times. The CFU mL^{-1} were graphed with error shown as ±SEM. All groups were compared with the untreated control group and significance was calculated using ordinary one-way ANOVA test with Dunnett's multiple comparisons test to generate corrected p values.

Microscopy imaging

K. pneumoniae NTUH K2044 Biofilms were seeded in 35 mm Matsunami glass-bottom culture dishes (VWR) with glass thickness of no. 1.5 (0.16–0.19 mm) and were treated

with peptide via the same specifications as the biofilm eradication assay. Following the 24-h treatment, the supernatant was removed, and the biofilms were washed with 1 mL of PBS. The biofilm polysaccharide matrix material was stained in 1 mL 0.1 M sodium bicarbonate with 100 mg mL^{-1} Texas red-conjugated concanavalin A (Invitrogen) for 5 min in the dark on a gel rocker. The dye was aspirated, and the samples were washed with 1 mL of PBS to remove residual dye. z stack images were taken with a Zeiss LSM 710 confocal microscope using a 63× oil objective with 488 and 543 nm laser channels. The figures shown are 3D renderings of the z stack images obtained to show the thickness of the biofilm on the z axis.

Mucoviscosity assay

To test for loss of the hypermucoviscous phenotype associated with extracellular polysaccharides, we tested the dispersed population for mucoviscosity as described previously.[33] We tested the untreated biofilm dispersed populations next to dispersed populations of biofilms treated with increasing concentrations of bac7 (1–35). Following removal of the supernatant from the biofilms, optical density was measured at 600 nm (OD_{600}) and compared with the OD_{600} of the samples after centrifugation for 5 min at 1,000 × *g*. These data were graphed as percent mucoviscosity following treatment, calculated by dividing the OD_{600} of the samples after centrifugation by the OD_{600} of the samples before centrifugation then multiplying the result by 100: $\%\ \text{Mucoviscosity} = \frac{(\text{OD 600 nm after centrifuge})}{(\text{OD 600 nm before centrifuge})} \times 100$. These data were analyzed for statistical significance using one-way ANOVA done using Tukey's multiple comparison test to adjust the resulting p values to correct for multiple comparisons.

Antimicrobial activity assays

K. pneumoniae NTUH K2044 were cultured on LB agar plates from frozen stocks and incubated overnight at 37°C. Next, one colony was selected and transferred to 6 mL of LB broth, and left to incubate overnight at 37°C. The next day, the bacterial cultures were diluted 1:100 in 6 mL of MHB and incubated at 37°C until the bacteria reached the logarithmic phase. The broth microdilution technique was used to determine the MIC values. This was done by introducing the peptides and the antibiotic polymyxin B (positive control), prepared as aqueous solutions in BSA buffer,[72] to non-treated polystyrene microtiter 96-well plate at a gradient of concentrations ranging from 0.0625 to 128 μmol L^{-1}. Next, a starting inoculum of 1×10^6 CFU mL^{-1} in MHB (LB was used for MIC testing to determine dosage for skin model) was added into the 96-well plate containing the peptide dilutions. After 24 h of incubation at 37°C, the lowest concentration of peptide that completely inhibited the growth of bacteria was identified as the MIC. The plates were read using a spectrophotometer to obtain the OD_{600}, and the assays were conducted in three independent replicates to ensure statistical reproducibility.

Extracellular polysaccharide extraction

K. pneumoniae NTUH K2044 was grown overnight in 500 mL of LB broth at 37°C with shaking. The overnight culture was then centrifuged at 18,800 × *g* at 4°C for 30 min and the pellet was resuspended in 10 mL of sterile water. For polysaccharide extraction, the hot phenol extraction method was used.[62] In brief, 10 mL of phenol was added to the

culture resuspended in water and incubated for 60 min in a 68°C water bath. Once cooled to room temperature, 10 mL of chloroform was added, and the extraction was centrifuged for 10 min at 4,000 × *g*. The aqueous layer was added to 3 volumes of ice-cold ethanol and stored in the −80°C freezer overnight. The extraction was then centrifuged at 4,000 × *g* for 10 min to pellet the polysaccharides. Once the supernatant was removed, the pellet was resuspended in 500 μL of sterile water and dialyzed overnight using a 100 Da dialysis membrane. The polysaccharides were then lyophilized and resuspended to 10 mg mL^{-1} in resuspension buffer (0.8% NaCl, 0.05% NaN_3 in 0.1 M Tris-HCl [pH 7]). To purify the polysaccharides two digestions were used: (1) to remove nucleotides, 5 μL of RNase A and 25 μL of DNase II type V were added to the sample and incubated for 18 h in a 37°C water bath and (2) to remove protein 2.5 μL of Proteinase K was added to the sample, incubated for 1 h at 55°C, and then at room temperature for 24 h. The purified sample was added to 5× volume of methanol with 1% (v/v) sodium acetate and centrifuged at 4,000 × *g* for 10 min to precipitate the polysaccharides. The supernatant was removed, and the sample was allowed to dry before resuspending in 5 mL sterile water. The sample was then subjected to two rounds of ultracentrifugation at 105,000 × *g* for 20 h each. The purified polysaccharide concentration was determined by uronic acid analysis.[73]

Extracellular biofilm polysaccharide analysis

Biofilm polysaccharides were extracted for analysis using a previously described method.[41] In brief, biofilms were grown by spotting 10 ¼L culture on Isopore 0.2 ¼m black PC membrane filters on LB agar and incubated for 48 h at 37°C. The biofilms were removed from the filters and resuspended in phosphate-buffered saline. The suspension was centrifuged at 48,000 × g at 4°C for 20 min and the resulting supernatant was filter sterilized using a 0.2 ¼m filter.

Purification processes—To remove free lipids, the dried extracts were suspended in 2 mL of nanopure water. Twenty milliliters of 95% ethanol was added to the suspension. The mixture was set at 4°C overnight, followed by centrifugation at 10,000 × g for 10 min. The sediment was dried under nitrogen flow. The sediment was resuspended in 4 mL 20 mM Tris-HCl (pH 8.0) with 20 μM of $MgCl_2$ and 0.1% (w/v) sodium azide, followed by addition of 2 μL benzonase (Sigma, E1014). The mixture was stirred at room temperature for 18 h. Twenty microliters of 6 μg/μL of protease K (Sigma, P2308) was added to the reaction. The mixture was heated at 50°C for 1 h, followed by stirring at room temperature overnight. The mixture was concentrated to 2 mL after lyophilization, and 14 mL of 95% ethanol was mixed with the suspension, which was kept at 4°C overnight. The mixture was centrifuged at 10,000 × *g* for 10 min. The supernatant was transferred to a new tube, dried under a stream of nitrogen, and referred to as Supernatant 1, while the precipitate was labeled Precipitate 1. Precipitate 1 was re-treated as Precipitate 2 to ensure complete removal of nucleic acid and protein components in the extract. The resulting supernatant and precipitate were referred to as Supernatant 2 and Precipitate 2, respectively.

1D ^{1}H-NMR analysis—An aliquot of 3.4 mg of the extract was dissolved in 550 μL of D_2O. One microliter of 50 mM DSS was added as internal standard. The solution was sonicated for 5 min and transferred into a 5 mm NMR tube. 1D ^{1}H-NMR spectra were

collected with a Bruker Avance III 600 MHz instrument equipped with a cryoprobe at 60°C for 64 scans. Analysis at high temperature is due to the milky status of the sample. The spectra were analyzed with MestReNova.

Glycosyl composition analysis by GC-MS of trimethylsilyl derivatives of methyl glycosides—Glycosyl composition analysis was performed by gas chromatography-mass spectrometry (GC-MS) of the per-*O*-trimethylsilyl (TMS) derivatives of the monosaccharide methyl glycosides generated from the samples by HCl methanolysis as described previously.[74] In brief, a 200–300 μg portion of each supernatant residue and precipitate was weighed and transferred into a glass screw-top tube, 20 μg of inositol was added as internal standard, and the mixture was lyophilized. Each sample was heated in 400 μL of 1 M methanolic HCl for 18 h at 80°C. After cooling and removal of the solvent under a stream of nitrogen, each sample was treated with a mixture of methanol, pyridine, and acetic anhydride for 30 min for N-acetylation. The solvents were evaporated, and each sample was derivatized with Tri-Sil HTP Reagent (Thermo Scientific) at 80°C for 30 min. Following extraction with hexane, GC-MS analysis of the TMS methyl glycosides was performed on an Agilent 7890A GC interfaced to a 5975C MSD, using a Supelco Equity-1 fused silica capillary column (30 m × 0.25 mm ID) employing a temperature gradient.

Glycosyl linkage analysis by GC-MS—Glycosyl linkage analysis was performed by combined GC-MS of the partially methylated alditol acetate (PMAA) derivatives produced from the sample. The procedure is a modification of the one described by Willis et al.[75] The lyophilized samples (470 μg) were suspended in 1-ethyl-3-methylimidazolium acetate with stirring for 2 days, followed by acetylation with acetic anhydride in the presence of 1-methylimidazole. The reaction was quenched by addition of nanopure water, and the acetylated materials were extracted from the water layer by dichloromethane (DCM). The dried DCM extract was stirred in 300 μL of anhydrous dimethyl sulfoxide (DMSO) for 1 day. Permethylation was achieved by three rounds of treatment with sodium hydroxide (NaOH) suspension (see below) and iodomethane, as follows. The NaOH base was prepared according to the protocol described by Anumula et al.[76] In brief, to NaOH (50%, w/w, 100 μL), methanol (200 μL, MeOH) was added, and the mixture was vortexed. Then DMSO (2 mL) was added, and the base solution was vortexed and centrifuged. The supernatant solution was removed and fresh DMSO was added. This was repeated 5 times. After the final extraction, DMSO (2 mL) was added to the NaOH pellet, and the solution was vortexed. Of this final base solution, 300 μL was added to the sample, and the mixture was magnetically stirred for 15 min. Then, iodomethane (70 μL) was added, and the sample was stirred at room temperature for 20 min. A second and third round of base (15 min) and then iodomethane (25 min) was added, the sample was then dissolved in DCM and washed 5 times with 2 mL of water. The water was removed, the remaining DCM dried off under a stream of nitrogen, and the sample was frozen and lyophilized. The permethylated materials were hydrolyzed with 2 M trifluoroacetic acid (TFA) for 2 h at 121°C and dried down with isopropanol under a stream of nitrogen. The samples were then reduced with $NaBD_4$ in nanopure water overnight, neutralized with glacial acetic acid, and dried with methanol. Finally, the samples were O-acetylated using acetic anhydride (250 μL) and concentrated TFA (250 μL) at 50°C for 20 min. The samples were dried under a stream of nitrogen,

reconstituted in DCM, and washed with nanopure water before injection into GC-MS. The resulting PMAAs were analyzed on an Agilent 7890A GC interfaced to a 5975C MSD; separation was performed on a Supelco 2331 fused silica capillary column (30 m × 0.25 mm ID) with a temperature gradient. The method is a derivation of the linkage method detailed by Black et al.[77]

Peptide:polysaccharide aggregation assays

The peptide aggregation with extracellular polysaccharides was performed using 300 μg mL^{-1} of extracted polysaccharide in 10 mM potassium phosphate buffer with 100 μmol L^{-1} of bac7 (1–35) analogs. The samples were then immediately centrifuged at 15,600 rpm for 15 min. The supernatant was removed following centrifugation, and the pellets were resuspended in 10 μL sterile water. The control for this experiment was included for the assessment of capsule retention to the microcentrifuge tubes and underwent centrifugation to assess aggregation of polysaccharide with no peptide. To assess the polysaccharides in the aggregates, the resuspended pellets were run on a 4%–8% bis-tris sodium dodecyl sulfate (SDS) page gel next to 2 μg of purified extracted polysaccharide for reference and stained with Alcian blue as described previously.[78] The aggregation was performed in triplicate and the gel images were analyzed for band density using ImageJ analysis software. The control band density was removed from all samples as background and the images were graphed reporting error as ± SEM.

Circular dichroism of bac7 (1–35) analogs

The peptides were assessed in the same buffer conditions used for the aggregation assessment to allow for a direct comparison. The analogs were resuspended at 100 μmol L^{-1} in 10 mM potassium phosphate buffer with or without 300 μg mL^{-1} of the extracted polysaccharides. The far UV (195–260 nm) spectra measurements were taken using a 0.1-cm pathlength quartz cuvette with the Jasco J-1500 CD spectrometer located in the Chemical Purification Analysis and Screening Core Facility at the University of South Florida. The samples were run with background corrected using either 10 mM potassium phosphate buffer or buffer with 300 μg mL^{-1} of the extracted polysaccharides. The resulting ellipticity data obtained were converted to mean residue ellipticity using the formula $\theta = \frac{(MRW * \theta)}{10 * d * c}$, where MRW is the mean residue weight of the peptides (molecular weight/#AA–1; #AA = number of amino acids), d is the pathlength of the cuvette, c is the concentration of the peptide, and Θ is the ellipticity in degrees.[79]

Ultraviolet photodissociation native mass spectrometry

Bac7 (1–35) and bac7 (10–35) solutions were prepared at 10 μmol L^{-1} in 5 mM ammonium acetate and spiked with 40 μmol L^{-1} stachyose hydrate (Sigma-Aldrich). High-resolution measurements for the peptide-oligosaccharide complexes were generated using a Thermo Scientific Orbitrap Fusion Lumos mass spectrometer coupled to a Coherent 193 nm excimer laser for UVPD in the high-pressure linear ion trap.[50,80] A Au/Pd-coated pulled static emitter was loaded with each stachyose peptide solution and individually infused into the mass spectrometer. The peptide · stachyose complexes (bac7 (1–35) in 5+ charge state and bac7 (10–35) in the 4+ charge state) were isolated and subjected to UVPD (1 laser

pulse at 3 mJ). The spectra were collected using a resolving power of 120 K at *m/z* 200 and deconvolved spectra were analyzed using MS-TAFI to calculate the yields of apo- and holo-fragment ions originating from backbone cleavages along each peptide using 10 ppm mass tolerance.[81] Apo fragment ions are standard peptide sequence ions that do not contain stachyose. Holo fragment ions are those that contain a portion of the peptide sequence plus stachyose. Holo-ion plots were generated by summing the abundances of all N-terminal (*a,b,c*) or C-terminal (*x,y,z*) holo-sequence ions originating from backbone cleavages across the peptide. For the differential plots, the fragmentation of the free peptide was analyzed in the presence and absence of stachyose (i.e., comparison of UVPD patterns of peptide versus peptide · stachyose). The abundances of fragment ions arising from backbone cleavages between each residue for the peptide without stachyose were subtracted from the fragment abundances for the corresponding peptide complex.

Hemolytic activity assays

Human red blood cells (RBCs) were purchased from ZenBio (blood type A^-). Blood samples were collected using heparin as an anti-coagulating agent. RBCs were washed with PBS (pH 7.4) 3 times using centrifugation at 800 × *g* for 10 min. To test the peptide's effects, aliquots of 200-fold diluted cells (75 μL) were mixed with peptide solutions (75 μL) in round-bottom cell-treated 96-well plates at concentrations ranging from 1 to 128 μmol L^{-1}, and incubated for 4 h at room temperature. After the incubation, the plates were centrifuged at 1,300 × *g* for 10 min to pellet the cells and debris, and 100 μL of the supernatant from each well was transferred to new, flat-bottom 96-well plates for absorbance reading at 405 nm. The percentage of hemolysis was calculated using the following equation: $\text{Hemolysis (\%)} = \frac{(\text{Abs405 nm treatment} - \text{Abs405 nm negative control})}{(\text{Abs405 nm positive control} - \text{Abs405 nm negative control})} \times 100$, where the negative control consisted of samples containing PBS, while the positive control consisted of samples containing 1% SDS in PBS (v/v).

Cytotoxic activity assays

HEK293T cells (human embryonic kidney cells) and HepG2 cells (immortalized liver cells) were cultured in high-glucose Dulbecco's modified Eagle's medium (DMEM) containing 1% penicillin/streptomycin and 10% fetal bovine serum (FBS). The cells were maintained at 37°C in a humidified atmosphere containing 5% CO_2. A day before treatment with increasing concentrations of peptide (ranging from 1 to 128 μmol L^{-1}), cells were seeded at a density of 5×10^3 cells per well into flat-bottom cell-treated 96-well plates. After 24 h of incubation with the peptides, the cell culture supernatants (100 μL per well) containing the peptides and cell solution were replaced with MTT reagent (0.5 mg mL^{-1}) in DMEM medium without phenol red. The samples were incubated for 4 h at 37°C to yield insoluble formazan salts. The salts were then solubilized with 0.04 mol L^{-1} HCl in anhydrous isopropanol and quantified using a spectrophotometer for absorbance reading at 550 nm. The percent killing was determined by the following equation: $\text{Percent killing} = \frac{(\text{Abs550 nm treatment} - \text{Abs550 nm negative control})}{(\text{Abs550 nm positive control} - \text{Abs550 nm negative control})} \times 100$. The negative control was water at the same volume as the peptide and the positive control was 1.0% Triton X-100 in water (v/v). The LD_{50} was then determined using the linear regression formula: $y = mx + b$.

Skin abscess mouse model

To assess the effectiveness of the peptides against *K. pneumoniae* NTUH K2044, bacterial cultures were grown in tryptic soy broth medium until an OD_{600} of 0.5 was reached. The cells were then washed with sterile PBS (pH 7.4) twice and resuspended with PBS to attain a final concentration of 5×10^6 CFU mL^{-1}. Next, female CD-1 mice, 6 weeks age, were anesthetized with isoflurane and subjected to a 1-cm-long superficial linear skin abrasion on their backs. Following this, a 20 μL aliquot containing bacterial load resuspended in PBS was inoculated over the abraded area. The peptides, diluted in water at their MIC, were administered to the infected area 1 h after the infection. Scarified skin areas were excised and homogenized using a bead beater (25 Hz) for 20 min and 10-fold serially diluted for CFU quantification. The animals were euthanized 2 and 4 days after infection, and skin samples were collected. Six mice per group (n = 6) were used for the experimental groups. The antibiotic polymyxin B was used as positive control. Statistical significance was determined using one-way ANOVA, p values are shown for each of the groups, all groups were compared with the untreated control group; features on the violin plots represent median and upper and lower quartiles.

Supplementary Material

Refer to Web version on PubMed Central for supplementary material.

ACKNOWLEDGMENTS

This work is supported by the National Institutes of Health R00AI163295 to R.M.F. and R35GM139658 and the Robert A. Welch Foundation (F-1155) to J.S.B. C.d.l.F.-N. holds a Presidential Professorship at the University of Pennsylvania and acknowledges funding from the Procter & Gamble Company, United Therapeutics, a BBRF Young Investigator Grant, the Nemirovsky Prize, Penn Health-Tech Accelerator Award, and the Dean's Innovation Fund from the Perelman School of Medicine at the University of Pennsylvania. Research reported in this publication was supported by the Langer Prize (AIChE Foundation), the National Institute of General Medical Sciences of the National Institutes of Health under award no. R35GM138201, and the Defense Threat Reduction Agency (DTRA) (HDTRA11810041, HDTRA1-21-1-0014, and HDTRA1-23-1-0001). The authors would like to thank Dr. Christian M. Harding for providing us with the NTUH K2044 *K. pneumoniae* isolate originating from Dr. Jose Bengoechea's lab at Queen's University Belfast. The authors also wish to acknowledge the contributions of Parastoo Azadi, Li Tan, and Christian Heiss in Figure S3 analysis of biofilm polysaccharides provided by the Complex Carbohydrate Research Center of the University of Georgia and supported by GlycoMIP, a National Science Foundation Materials Innovation Platform funded through cooperative agreement DMR-1933525.

DECLARATION OF INTERESTS

C.d.l.F.-N. provides consulting services to Invaio Sciences and is a member of the scientific advisory boards of Nowture S.L. and Phare Bio. The de la Fuente lab has received research funding or in-kind donations from United Therapeutics, Strata Manufacturing PJSC, and Procter & Gamble, none of which were used in support of this work. C.d.l.F.-N. is on the advisory board of *Cell Reports Physical Science*.

REFERENCES

1. Marsh JW, Mustapha MM, Griffith MP, Evans DR, Ezeonwuka C, Pasculle AW, Shutt KA, Sundermann A, Ayres AM, Shields RK, et al. (2019). Evolution of Outbreak-Causing Carbapenem-Resistant *Klebsiella pneumoniae* ST258 at a Tertiary Care Hospital over 8 Years. mBio 10, e01945–19. 10.1128/mBio.01945-19. [PubMed: 31481386]
2. Caneiras C, Lito L, Melo-Cristino J, and Duarte A (2019). Community- and Hospital-Acquired *Klebsiella pneumoniae* Urinary Tract Infections in Portugal: Virulence and Antibiotic Resistance. Microorganisms 7, 138. 10.3390/microorganisms7050138. [PubMed: 31100810]

3. Onori R, Gaiarsa S, Comandatore F, Pongolini S, Brisse S, Colombo A, Cassani G, Marone P, Grossi P, Minoja G, et al. (2015). Tracking Nosocomial *Klebsiella pneumoniae* Infections and Outbreaks by Whole-Genome Analysis: Small-Scale Italian Scenario within a Single Hospital. J. Clin. Microbiol 53, 2861–2868. 10.1128/JCM.00545-15. [PubMed: 26135860]
4. Al Bshabshe A, Al-Hakami A, Alshehri B, Al-Shahrani KA, Alshehri AA, Al Shahrani MB, Assiry I, Joseph MR, Alkahtani A, and Hamid ME (2020). Rising *Klebsiella pneumoniae* Infections and Its Expanding Drug Resistance in the Intensive Care Unit of a Tertiary Healthcare Hospital, Saudi Arabia. Cureus 12, e10060. 10.7759/cureus.10060. [PubMed: 32999783]
5. Yahya RO (2022). Problems Associated with Co-Infection by Multidrug-Resistant *Klebsiella pneumoniae* in COVID-19 Patients: A Review. Healthcare (Basel) 10, 2412. 10.3390/healthcare10122412. [PubMed: 36553936]
6. Effah CY, Sun T, Liu S, and Wu Y (2020). *Klebsiella pneumoniae*: an increasing threat to public health. Ann. Clin. Microbiol. Antimicrob 19, 1. 10.1186/s12941-019-0343-8. [PubMed: 31918737]
7. Bengoechea JA, and Sa Pessoa J (2019). *Klebsiella pneumoniae* infection biology: living to counteract host defences. FEMS Microbiol. Rev 43, 123–144. 10.1093/femsre/fuy043. [PubMed: 30452654]
8. Gonzalez-Ferrer S, Peñaloza HF, Budnick JA, Bain WG, Nordstrom HR, Lee JS, and Van Tyne D (2021). Finding Order in the Chaos: Outstanding Questions in *Klebsiella pneumoniae* Pathogenesis. Infect. Immun 89, e00693–20. 10.1128/IAI.00693-20. [PubMed: 33558323]
9. Kot B, Piechota M, Szweda P, Mitrus J, Wicha J, Grużewska A, and Witeska M (2023). Virulence analysis and antibiotic resistance of *Klebsiella pneumoniae* isolates from hospitalised patients in Poland. Sci. Rep 13, 4448. 10.1038/s41598-023-31086-w. [PubMed: 36932105]
10. Martin MJ, Corey BW, Sannio F, Hall LR, MacDonald U, Jones BT, Mills EG, Harless C, Stam J, Maybank R, et al. (2021). Anatomy of an extensively drug-resistant *Klebsiella pneumoniae* outbreak in Tuscany, Italy. Proc. Natl. Acad. Sci. USA 118, e2110227118. 10.1073/pnas.2110227118. [PubMed: 34819373]
11. Navon-Venezia S, Kondratyeva K, and Carattoli A (2017). *Klebsiella pneumoniae*: a major worldwide source and shuttle for antibiotic resistance. FEMS Microbiol. Rev 41, 252–275. 10.1093/femsre/fux013. [PubMed: 28521338]
12. Eger E, Schwabe M, Schulig L, Hübner NO, Bohnert JA, Bornscheuer UT, Heiden SE, Müller JU, Adnan F, Becker K, et al. (2022). Extensively Drug-Resistant *Klebsiella pneumoniae* Counteracts Fitness and Virulence Costs That Accompanied Ceftazidime-Avibactam Resistance Acquisition. Microbiol. Spectr 10, e0014822. 10.1128/spectrum.00148-22. [PubMed: 35435751]
13. Martin MJ, Stribling W, Ong AC, Maybank R, Kwak YI, Rosado-Mendez JA, Preston LN, Lane KF, Julius M, Jones AR, et al. (2023). A panel of diverse *Klebsiella pneumonia* clinical isolates for research and development. Microb. Genom 9, mgen000967. 10.1099/mgen.0.000967. [PubMed: 37141116]
14. Russo TA, and Marr CM (2019). Hypervirulent *Klebsiella pneumoniae*. Clin. Microbiol. Rev 32, e00001–19. 10.1128/CMR.00001-19. [PubMed: 31092506]
15. Choby JE, Howard-Anderson J, and Weiss DS (2020). Hypervirulent *Klebsiella pneumoniae* - clinical and molecular perspectives. J. Intern. Med 287, 283–300. 10.1111/joim.13007. [PubMed: 31677303]
16. Shon AS, Bajwa RPS, and Russo TA (2013). Hypervirulent (hypermucoviscous) *Klebsiella pneumoniae*: a new and dangerous breed. Virulence 4, 107–118. 10.4161/viru.22718. [PubMed: 23302790]
17. Sanchez-Lopez J, Garcia-Caballero A, Navarro-San Francisco C, Quereda C, Ruiz-Garbajosa P, Navas E, Dronda F, Morosini MI, Canton R, and Diez-Aguilar M (2019). Hypermucoviscous *Klebsiella pneumoniae*: A challenge in community acquired infection. IDCases 17, e00547. 10.1016/j.idcr.2019.e00547. [PubMed: 31193033]
18. Mike LA, Stark AJ, Forsyth VS, Vornhagen J, Smith SN, Bachman MA, and Mobley HLT (2021). A systematic analysis of hypermucoviscosity and capsule reveals distinct and overlapping genes that impact *Klebsiella pneumoniae* fitness. PLoS Pathog. 17, e1009376. 10.1371/journal.ppat.1009376. [PubMed: 33720976]

19. de la Fuente-Nunez C, Reffuveille F, Fernandez L, and Hancock RE (2013). Bacterial biofilm development as a multicellular adaptation: antibiotic resistance and new therapeutic strategies. Curr. Opin. Microbiol 16, 580–589. 10.1016/j.mib.2013.06.013. [PubMed: 23880136]
20. Karygianni L, Ren Z, Koo H, and Thurnheer T (2020). Biofilm Matrixome: Extracellular Components in Structured Microbial Communities. Trends Microbiol. 28, 668–681. 10.1016/j.tim.2020.03.016. [PubMed: 32663461]
21. Limoli DH, Jones CJ, and Wozniak DJ (2015). Bacterial Extracellular Polysaccharides in Biofilm Formation and Function. Microbiol. Spectr 3. 10.1128/microbiolspec.MB-0011-2014.
22. Koo H, Xiao J, and Klein MI (2009). Extracellular polysaccharides matrix–an often forgotten virulence factor in oral biofilm research. Int. J. Oral Sci 1, 229–234. 10.4248/IJOS.09086. [PubMed: 20690427]
23. Vuotto C, Longo F, Balice MP, Donelli G, and Varaldo PE (2014). Antibiotic Resistance Related to Biofilm Formation in *Klebsiella pneumoniae*. Pathogens 3, 743–758. 10.3390/pathogens3030743. [PubMed: 25438022]
24. Wang G, Zhao G, Chao X, Xie L, and Wang H (2020). The Characteristic of Virulence, Biofilm and Antibiotic Resistance of *Klebsiella pneumoniae*. Int. J. Environ. Res. Public Health 17, 6278. 10.3390/ijerph17176278. [PubMed: 32872324]
25. Pfalzgraff A, Brandenburg K, and Weindl G (2018). Antimicrobial Peptides and Their Therapeutic Potential for Bacterial Skin Infections and Wounds. Front. Pharmacol 9, 281. 10.3389/fphar.2018.00281. [PubMed: 29643807]
26. Gera S, Kankuri E, and Kogermann K (2022). Antimicrobial peptides - Unleashing their therapeutic potential using nanotechnology. Pharmacol. Ther 232, 107990. 10.1016/j.pharmthera.2021.107990. [PubMed: 34592202]
27. Bayramov D, Li Z, Patel E, Izadjoo M, Kim H, and Neff J (2018). A Novel Peptide-Based Antimicrobial Wound Treatment is Effective Against Biofilms of Multi-Drug Resistant Wound Pathogens. Mil. Med 183, 481–486. 10.1093/milmed/usx135. [PubMed: 29635548]
28. de la Fuente-Nunez C, Korolik V, Bains M, Nguyen U, Breidenstein EB, Horsman S, Lewenza S, Burrows L, and Hancock RE (2012). Inhibition of bacterial biofilm formation and swarming motility by a small synthetic cationic peptide. Antimicrob. Agents Chemother 56, 2696–2704. 10.1128/AAC.00064-12. [PubMed: 22354291]
29. Cesaro A, Torres MDT, Gaglione R, Dell'Olmo E, Di Girolamo R, Bosso A, Pizzo E, Haagsman HP, Veldhuizen EJA, de la Fuente-Nunez C, and Arciello A (2022). Synthetic Antibiotic Derived from Sequences Encrypted in a Protein from Human Plasma. ACS Nano 16, 1880–1895. 10.1021/acsnano.1c04496. [PubMed: 35112568]
30. de la Fuente-Nunez C, Cardoso MH, de Souza Candido E, Franco OL, and Hancock RE (2016). Synthetic antibiofilm peptides. Biochim. Biophys. Acta 1858, 1061–1069. 10.1016/j.bbamem.2015.12.015. [PubMed: 26724202]
31. Ribeiro SM, de la Fuente-Núñez C, Baquir B, Faria-Junior C, Franco OL, and Hancock REW (2015). Antibiofilm peptides increase the susceptibility of carbapenemase-producing *Klebsiella pneumoniae* clinical isolates to beta-lactam antibiotics. Antimicrob. Agents Chemother 59, 3906–3912. 10.1128/AAC.00092-15. [PubMed: 25896694]
32. Fleeman RM, Macias LA, Brodbelt JS, and Davies BW (2020). Defining principles that influence antimicrobial peptide activity against capsulated *Klebsiella pneumoniae*. Proc. Natl. Acad. Sci. USA 117, 27620–27626. 10.1073/pnas.2007036117. [PubMed: 33087568]
33. Fleeman RM, and Davies BW (2022). Polyproline Peptide Aggregation with *Klebsiella pneumoniae* Extracellular Polysaccharides Exposes Biofilm Associated Bacteria. Microbiol. Spectr 10, e0202721. 10.1128/spectrum.02027-21. [PubMed: 35254120]
34. Mardirossian M, Grzela R, Giglione C, Meinnel T, Gennaro R, Mergaert P, and Scocchi M (2014). The host antimicrobial peptide Bac71-35 binds to bacterial ribosomal proteins and inhibits protein synthesis. Chem. Biol 21, 1639–1647. 10.1016/j-chembiol.2014.10.009. [PubMed: 25455857]
35. Runti G, Benincasa M, Giuffrida G, Devescovi G, Venturi V, Gennaro R, and Scocchi M (2017). The Mechanism of Killing by the Proline-Rich Peptide Bac7(1-35) against Clinical Strains of Pseudomonas aeruginosa Differs from That against Other Gram-Negative Bacteria. Antimicrob. Agents Chemother 61, e01660–16. 10.1128/AAC.01660-16. [PubMed: 28137800]

36. Sutherland I. (1990). Biotechnology of Microbial Exopolysaccharides (Cambridge Studies in Biotechnology), C.C.U. Press, ed. (Cambrige University Press). 10.1017/CBO9780511525384.
37. McSwain BS, Irvine RL, Hausner M, and Wilderer PA (2005). Composition and distribution of extracellular polymeric substances in aerobic flocs and granular sludge. Appl. Environ. Microbiol 71, 1051–1057. 10.1128/AEM.71.Z1051-1057.2005. [PubMed: 15691965]
38. Kolodkin-Gal I, Cao S, Chai L, Böttcher T, Kolter R, Clardy J, and Losick R (2012). A self-produced trigger for biofilm disassembly that targets exopolysaccharide. Cell 149, 684–692. 10.1016/j.cell.2012.02.055. [PubMed: 22541437]
39. Benincasa M, Scocchi M, Podda E, Skerlavaj B, Dolzani L, and Gennaro R (2004). Antimicrobial activity of Bac7 fragments against drug-resistant clinical isolates. Peptides 25, 2055–2061. 10.1016/j.peptides.2004.08.004. [PubMed: 15572192]
40. Seefeldt AC, Graf M, Pérébaskine N, Nguyen F, Arenz S, Mardirossian M, Scocchi M, Wilson DN, and Innis CA (2016). Structure of the mammalian antimicrobial peptide Bac7(1-16) bound within the exit tunnel of a bacterial ribosome. Nucleic Acids Res. 44, 2429–2438. 10.1093/nar/gkv1545. [PubMed: 26792896]
41. Benincasa M, Lagatolla C, Dolzani L, Milan A, Pacor S, Liut G, Tossi A, Cescutti P, and Rizzo R (2016). Biofilms from *Klebsiella pneumoniae*: Matrix Polysaccharide Structure and Interactions with Antimicrobial Peptides. Microorganisms 4, 26. 10.3390/microorganisms4030026. [PubMed: 27681920]
42. Chin DH, Woody RW, Rohl CA, and Baldwin RL (2002). Circular dichroism spectra of short, fixed-nucleus alanine helices. Proc. Natl. Acad. Sci. USA 99, 15416–15421. 10.1073/pnas.232591399. [PubMed: 12427967]
43. Allison TM, and Bechara C (2019). Structural mass spectrometry comes of age: new insight into protein structure, function and interactions. Biochem. Soc. Trans 47, 317–327. 10.1042/BST20180356. [PubMed: 30647140]
44. Chait BT, Cadene M, Olinares PD, Rout MP, and Shi Y (2016). Revealing Higher Order Protein Structure Using Mass Spectrometry. J. Am. Soc. Mass Spectrom 27, 952–965. 10.1007/s13361-016-1385-1. [PubMed: 27080007]
45. Konijnenberg A, Butterer A, and Sobott F (2013). Native ion mobility-mass spectrometry and related methods in structural biology. Biochim. Biophys. Acta 1834, 1239–1256. 10.1016/j.bbapap.2012.11.013. [PubMed: 23246828]
46. Leney AC, and Heck AJR (2017). Native Mass Spectrometry: What is in the Name? J. Am. Soc. Mass Spectrom 28, 5–13. 10.1021/jasms.8b05378.
47. Mehmood S, Allison TM, and Robinson CV (2015). Mass Spectrometry of Protein Complexes: From Origins to Applications. Annu. Rev. Phys. Chem 66, 453–474. 10.1146/annurev-physchem-040214-121732. [PubMed: 25594852]
48. Cammarata MB, Schardon CL, Mehaffey MR, Rosenberg J, Singleton J, Fast W, and Brodbelt JS (2016). Impact of G12 Mutations on the Structure of K-Ras Probed by Ultraviolet Photodissociation Mass Spectrometry. J. Am. Chem. Soc 138, 13187–13196. 10.1021/jacs.6b04474. [PubMed: 27665622]
49. Cammarata MB, Thyer R, Rosenberg J, Ellington A, and Brodbelt JS (2015). Structural Characterization of Dihydrofolate Reductase Complexes by Top-Down Ultraviolet Photodissociation Mass Spectrometry. J. Am. Chem. Soc 137, 9128–9135. 10.1021/jacs.5b04628. [PubMed: 26125523]
50. Crittenden CM, Morrison LJ, Fitzpatrick MD, Myers AP, Novelli ET, Rosenberg J, Akin LD, Srinivasa S, Shear JB, and Brodbelt JS (2018). Towards mapping electrostatic interactions between Kdo2-lipid A and cationic antimicrobial peptides via ultraviolet photodissociation mass spectrometry. Analyst 143, 3607–3618. 10.1039/c8an00652k. [PubMed: 29968868]
51. Mehaffey MR, Cammarata MB, and Brodbelt JS (2018). Tracking the Catalytic Cycle of Adenylate Kinase by Ultraviolet Photodissociation Mass Spectrometry. Anal. Chem 90, 839–846. 10.1021/acs.analchem.7b03591. [PubMed: 29188992]
52. O'Brien JP, Li W, Zhang Y, and Brodbelt JS (2014). Characterization of native protein complexes using ultraviolet photodissociation mass spectrometry. J. Am. Chem. Soc 136, 12920–12928. 10.1021/ja505217w. [PubMed: 25148649]

53. Rosenberg J, Parker WR, Cammarata MB, and Brodbelt JS (2018). UV-POSIT: Web-Based Tools for Rapid and Facile Structural Interpretation of Ultraviolet Photodissociation (UVPD) Mass Spectra. J. Am. Soc. Mass Spectrom 29, 1323–1326. 10.1007/s13361-018-1918-x. [PubMed: 29626295]
54. Sipe SN, and Brodbelt JS (2019). Impact of charge state on 193 nm ultraviolet photodissociation of protein complexes. Phys. Chem. Chem. Phys 21, 9265–9276. 10.1039/C9CP01144G. [PubMed: 31016301]
55. Torres MDT, Melo MCR, Flowers L, Crescenzi O, Notomista E, and de la Fuente-Nunez C (2022). Mining for encrypted peptide antibiotics in the human proteome. Nat. Biomed. Eng 6, 67–75. 10.1038/s41551-021-00801-1. [PubMed: 34737399]
56. Boaro A, Ageitos L, Torres MDT, Blasco EB, Oztekin S, and de la Fuente-Nunez C (2023). Structure-function-guided design of synthetic peptides with anti-infective activity derived from wasp venom. Cell Rep. Phys. Sci 4, 101459. 10.1016/j.xcrp.2023.101459. [PubMed: 38239869]
57. Torres MDT, Pedron CN, Higashikuni Y, Kramer RM, Cardoso MH, Oshiro KGN, Franco OL, Silva Junior PI, Silva FD, Oliveira Junior VX, et al. (2018). Structure-function-guided exploration of the antimicrobial peptide polybia-CP identifies activity determinants and generates synthetic therapeutic candidates. Commun. Biol 1, 221. 10.1038/s42003-018-0224-2. [PubMed: 30534613]
58. Maasch JRMA, Torres MDT, Melo MCR, and de la Fuente-Nunez C (2023). Molecular de-extinction of ancient antimicrobial peptides enabled by machine learning. Cell Host Microbe 31, 1260–1274.e6. 10.1016/j.chom.2023.07.001. [PubMed: 37516110]
59. Silveira GGOS, Torres MDT, Ribeiro CFA, Meneguetti BT, Carvalho CME, de la Fuente-Nunez C, Franco OL, and Cardoso MH (2021). Antibiofilm Peptides: Relevant Preclinical Animal Infection Models and Translational Potential. ACS Pharmacol. Transl. Sci 4, 55–73. 10.1021/acsptsci.0c00191. [PubMed: 33615161]
60. Sen CK, Roy S, Mathew-Steiner SS, and Gordillo GM (2021). Biofilm Management in Wound Care. Plast. Reconstr. Surg 148, 275e–288e. 10.1097/PRS.0000000000008142.
61. Clinton A, and Carter T (2015). Chronic Wound Biofilms: Pathogenesis and Potential Therapies. Lab. Med 46, 277–284. 10.1309/LMBNSWKUI4JPN7SO. [PubMed: 26489671]
62. Campos MA, Vargas MA, Regueiro V, Llompart CM, Albertí S, and Bengoechea JA (2004). Capsule polysaccharide mediates bacterial resistance to antimicrobial peptides. Infect. Immun 72, 7107–7114. 10.1128/IAI.72.12.7107-7114.2004. [PubMed: 15557634]
63. Bengoechea JA, and Sa Pessoa J (2019). *Klebsiella pneumoniae* infection biology: living to counteract host defences. FEMS Microbiol. Rev 43, 123–144. 10.1093/femsre/fuy043. [PubMed: 30452654]
64. Adzhubei AA, Sternberg MJE, and Makarov AA (2013). Polyproline-II helix in proteins: structure and function. J. Mol. Biol 425, 2100–2132. 10.1016/j.jmb.2013.03.018. [PubMed: 23507311]
65. Kay BK, Williamson MP, and Sudol M (2000). The importance of being proline: the interaction of proline-rich motifs in signaling proteins with their cognate domains. FASEB J 14, 231–241. [PubMed: 10657980]
66. Zondlo NJ (2013). Aromatic-proline interactions: electronically tunable CH/pi interactions. Acc. Chem. Res 46, 1039–1049. 10.1021/ar300087y. [PubMed: 23148796]
67. Choby JE, Howard-Anderson J, and Weiss DS (2020). Hypervirulent *Klebsiella pneumoniae*–clinical and molecular perspectives. J. Intern. Med 287, 283–300. 10.1111/joim.13007. [PubMed: 31677303]
68. Nang SC, Han ML, Yu HH, Wang J, Torres VVL, Dai C, Velkov T, Harper M, and Li J (2019). Polymyxin resistance in *Klebsiella pneumoniae*: multifaceted mechanisms utilized in the presence and absence of the plasmid-encoded phosphoethanolamine transferase gene mcr-1. J. Antimicrob. Chemother 74, 3190–3198. 10.1093/jac/dkz314. [PubMed: 31365098]
69. Bartolleti F, Seco BMS, Capuzzo Dos Santos C, Felipe CB, Lemo MEB, Alves T.d.S., Passadore LF, Mimica MJ, Sampaio SCF, Zavascki AP, and Sampaio JLM (2016). Polymyxin B Resistance in Carbapenem-Resistant *Klebsiella pneumoniae*, Sao Paulo, Brazil. Emerg. Infect. Dis 22, 1849–1851. 10.3201/eid2210.160695. [PubMed: 27648951]

70. Nivens DE, Ohman DE, Williams J, and Franklin MJ (2001). Role of alginate and its O acetylation in formation of *Pseudomonas aeruginosa* microcolonies and biofilms. J. Bacteriol 183, 1047–1057. 10.1128/JB.183.3.1047-1057.2001. [PubMed: 11208804]
71. Jumper J, Evans R, Pritzel A, Green T, Figurnov M, Ronneberger O, Tunyasuvunakool K, Bates R, Žídek A, Potapenko A, et al. (2021). Highly accurate protein structure prediction with AlphaFold. Nature 596, 583–589. 10.1038/s41586-021-03819-2. [PubMed: 34265844]
72. Wiegand I, Hilpert K, and Hancock REW (2008). Agar and broth dilution methods to determine the minimal inhibitory concentration (MIC) of antimicrobial substances. Nat. Protoc 3, 163–175. 10.1038/nprot.2007.521. [PubMed: 18274517]
73. Brimacombe C, and Beatty J (2013). Surface Polysaccharide Extraction and Quantification. Bio-Protocol 3. 10.21769/BioProtoc.934.
74. Santander J, Martin T, Loh A, Pohlenz C, Gatlin DM, and Curtiss R (2013). Mechanisms of intrinsic resistance to antimicrobial peptides of *Edwardsiella ictaluri* and its influence on fish gut inflammation and virulence. Microbiology (Read.) 159, 1471–1486. 10.1099/mic.0O66639-0.
75. Willis LM, Stupak J, Richards MR, Lowary TL, Li J, and Whitfield C (2013). Conserved glycolipid termini in capsular polysaccharides synthesized by ATP-binding cassette transporter-dependent pathways in Gram-negative pathogens. Proc. Natl. Acad. Sci. USA 110, 7868–7873 10.1073/pnas.1222317110. [PubMed: 23610430]
76. Anumula KR, and Taylor PB (1992). A comprehensive procedure for preparation of partially methylated alditol acetates from glycoprotein carbohydrates. Anal. Biochem 203, 101–108. 10.1016/0003-2697(92)90048-c. [PubMed: 1524204]
77. Black IM, Ndukwe IE, Vlach J, Backe J, Urbanowicz BR, Heiss C, and Azadi P (2023). Acetylation in Ionic Liquids Dramatically Increases Yield in the Glycosyl Composition and Linkage Analysis of Insoluble and Acidic Polysaccharides. Anal. Chem 95, 12851–12858. 10.1021/acs.analchem.3c02056. [PubMed: 37595025]
78. Karlyshev AV, and Wren BW (2001). Detection and Initial Characterization of Novel Capsular Polysaccharide among Diverse *Campylobacter jejuni* Strains Using Alcian Blue Dye. J. Clin. Microbiol 39, 279–284. 10.1128/jcm.39.1.279-284.2001. [PubMed: 11136784]
79. Kelly SM, Jess TJ, and Price NC (2005). How to study proteins by circular dichroism. Biochim. Biophys. Acta 1751, 119–139. 10.1016/j.bbapap.2005.06.005. [PubMed: 16027053]
80. Klein DR, Holden DD, and Brodbelt JS (2016). Shotgun Analysis of Rough-Type Lipopolysaccharides Using Ultraviolet Photodissociation Mass Spectrometry. Anal. Chem 88, 1044–1051. 10.1021/acs.analchem.5b04218. [PubMed: 26616388]
81. Juetten KJ, and Brodbelt JS (2023). MS-TAFI: A Tool for the Analysis of Fragment Ions Generated from Intact Proteins. J. Proteome Res 22, 546–550. 10.1021/acs.jproteome.2c00594. [PubMed: 36516971]

Highlights

- Confocal imaging visualizes the released cells and collapse of the biofilm matrix
- Truncated analogs reveal polysaccharide interactions drive the matrix disruption
- Mass spectrometry describes the polysaccharide interaction region of bac7 (1–35)
- Topical application using a skin abscess model decreases the bacterial burden *in vivo*

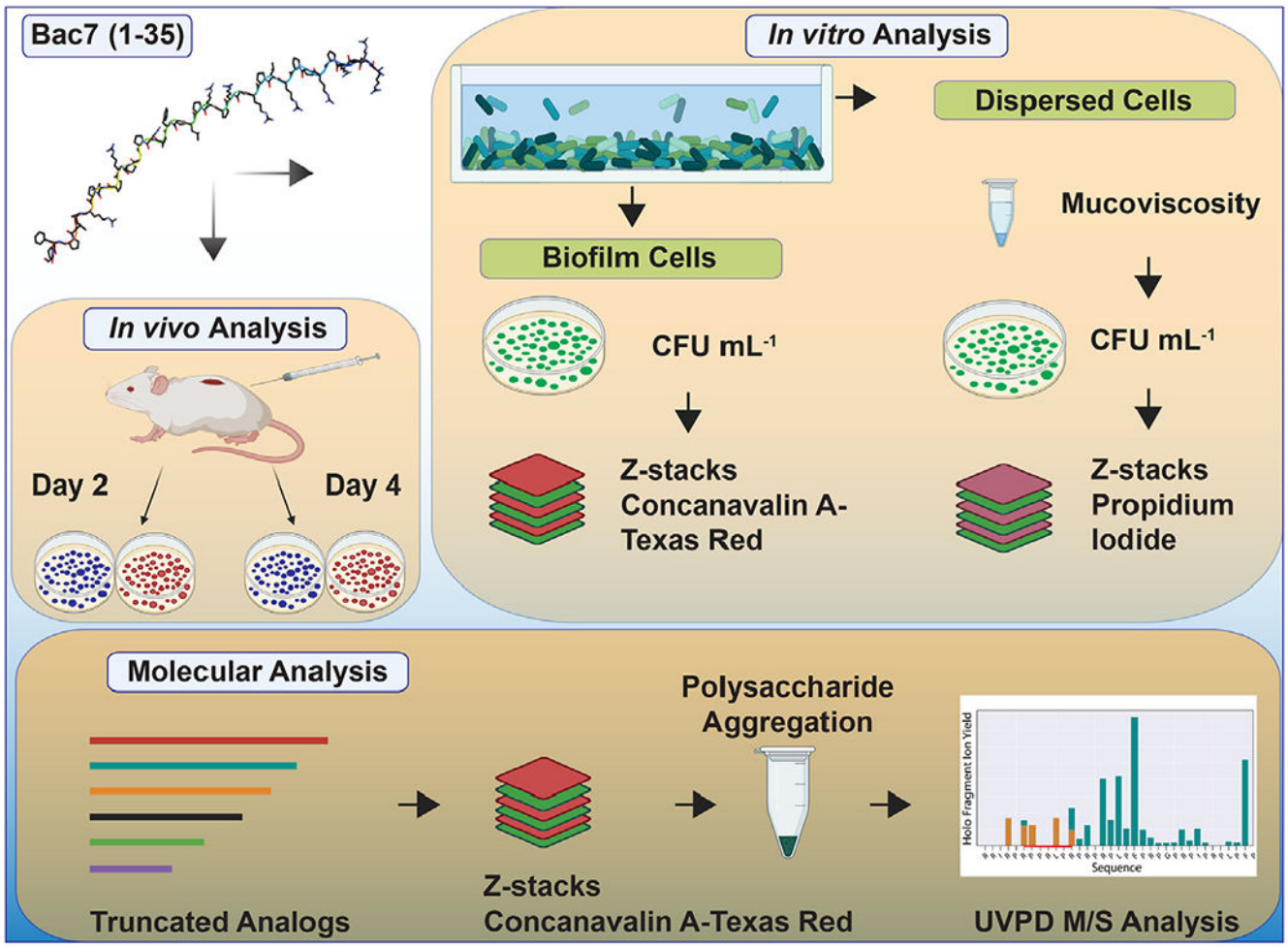

Figure 1. Workflow of the multi-level biofilm analysis

The figure shows the multi-level approach to understanding bac7 (1–35) biofilm disruption capabilities. The structure of bac7 (1–35) is shown in the upper left corner with arrows pointing to the division of *in vitro* and *in vivo* work. *In vitro* analysis included assessment of the biofilm cells and the dispersed planktonic population. The bottom panel shows the molecular analysis done with bac7 (1–35) and truncated analogs to determine the polysaccharide interactions. AlphaFold was used to create the bac7 (1–35) peptide, BioRender was used for the vector production, and Adobe Illustrator was used to construct the final figure.

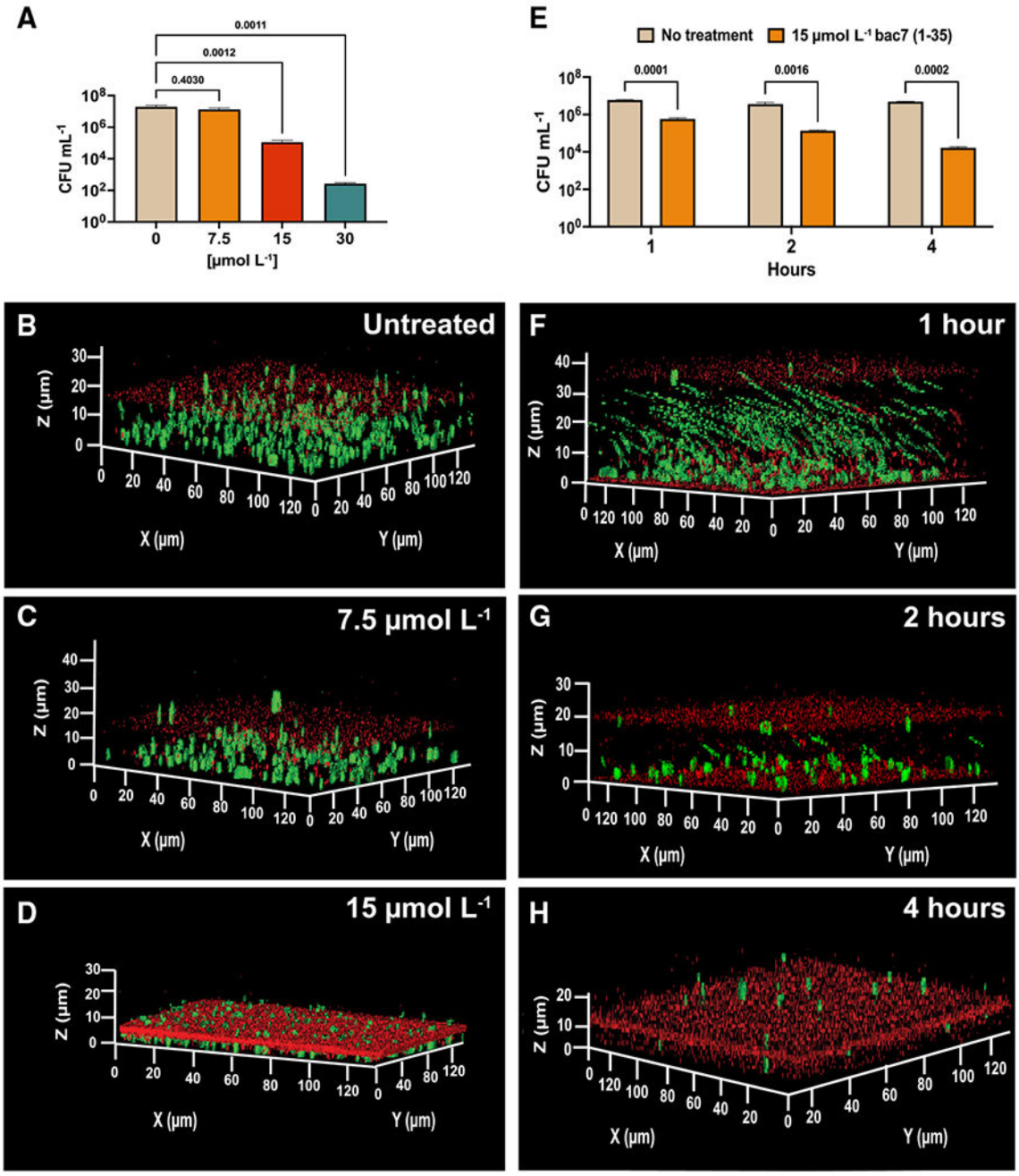

Figure 2. Bac7 (1-35) treatment induces matrix polysaccharide collapse and release of biofilm-associated cells

The figure shows the enumeration of *K. pneumoniae* NTUH K2044 biofilms next to 3D rendering of the z stack images of the biofilms formed by hypervirulent *K. pneumoniae* NTUH K2044 constitutively expressing GFP and matrix polysaccharides stained with Texas red-conjugated concanavalin A.

(A) TheCFU mL^{-1} of the biofilm following treatment with 0, 7.5, 15, and 30 μmol L^{-1} of bac7 (1–35).

(B) The z stack images with three scale bars z, x, and y (μm) of the non-treated biofilm.

(C and D) The biofilms treated with 7.5 and 15 μmol L^{-1} of bac7 (1–35), respectively.
(E) The corresponding CFU mL^{-1} counts for the short time points tested with 15 μmol L^{-1} of bac7 (1–35).
(F) The release of the upper layers of the biofilm after 1 h treatment.
(G) The decrease of matrix associated cells after 2 h.
(H) Complete collapse of the biofilm matrix after 4 h treatment with bac7 (1–35). n = 3 biofilms were grown and imaged for the controls and bac7 (1–35) treatment and representative images are shown for each concentration. (A) and (E) were graphed as mean values with error shown as ± SEM and statistical analyses were done comparing peptide treatment to untreated controls using ordinary one-way ANOVA with Dunnett's multiple comparisons test to correct for multiple comparisons and provide the adjusted p values displayed on the graphs.

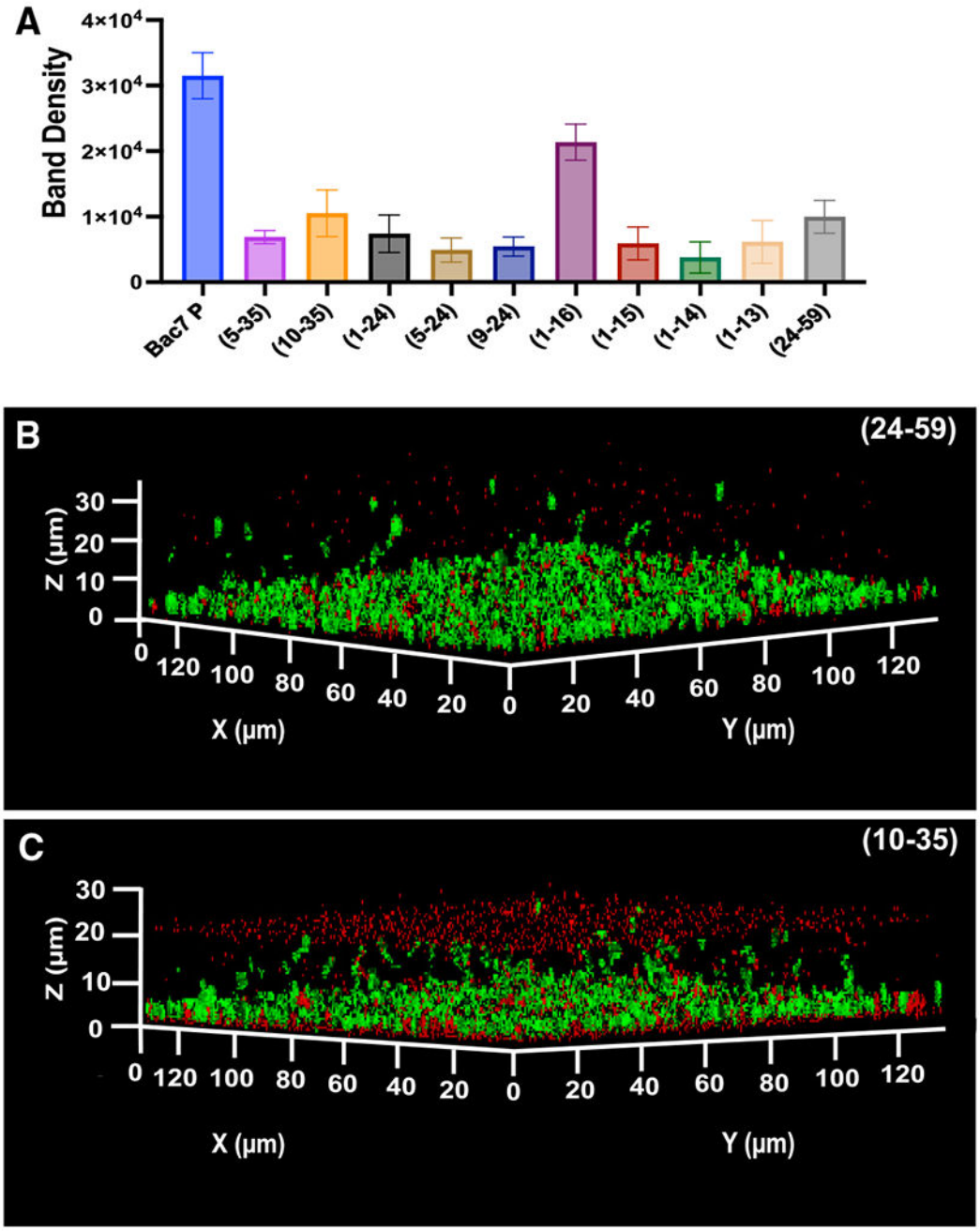

Figure 3. Biofilm matrix modulation by bac7 (1–35) analogs is not correlated with antimicrobial activity but extracellular polysaccharide interactions

The figures show polysaccharide aggregation of the analogs and the 3D rendering of the z stack images of biofilms treated with the antimicrobial inactive analogs bac7 (24–59) and bac7 (10–35).

(A) The band density quantification of polysaccharide aggregates from the SDS-PAGE (Figure S3) used to generate the extracellular polysaccharide relative aggregation potential for Table 1.

(B and C) The biofilms after 24 h treatment with 60 μmol L^{-1} of bac7 (24–59) and bac7 (10–35), respectively. n = 3 biofilms were grown, and representative images are shown for each peptide.

(A) aggregation was done in triplicate with a representative gel shown in Figure S3H and ImageJ analysis was used to quantify and graph the mean data with error shown as ± SEM.

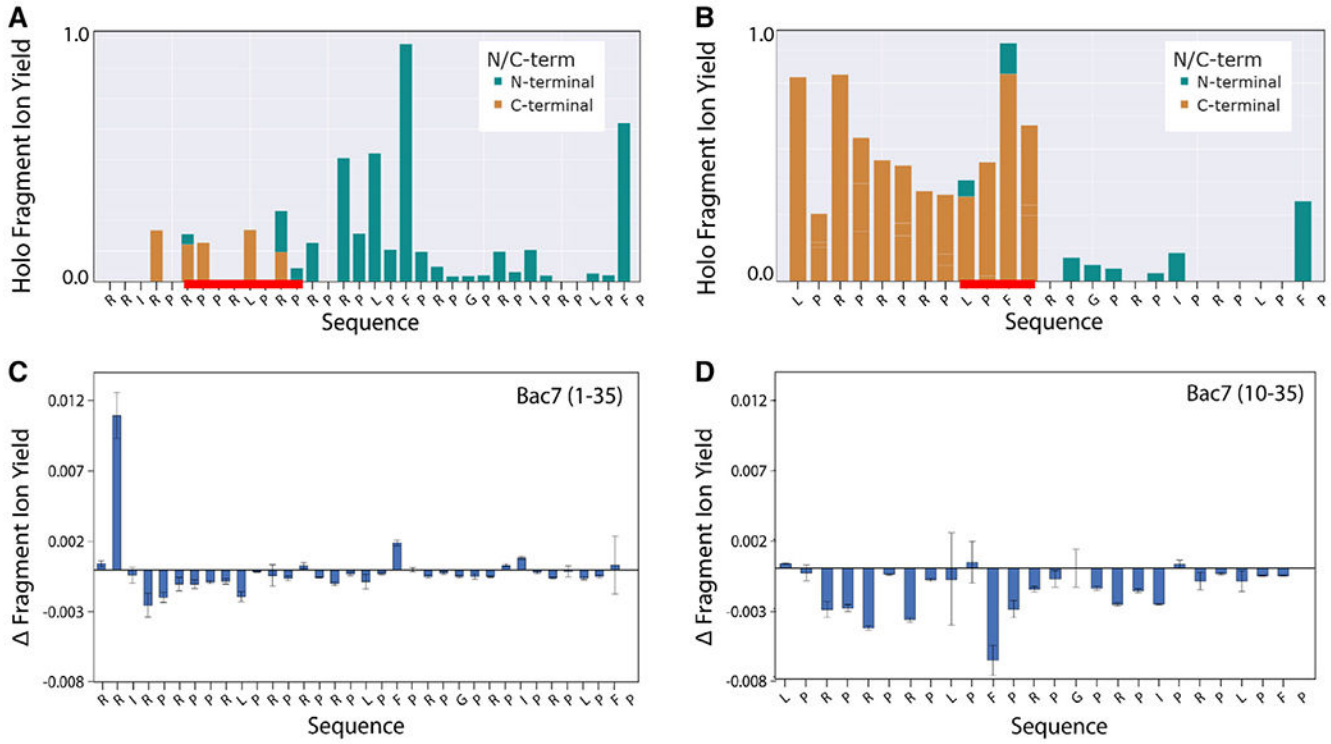

Figure 4. UVPD native mass spectrometry reveals that interactions with stachyose drive the loss of peptide structure

The bar graphs in (A) and (B) show the series of holo fragment ions for bac7 (1–35) • stachyose (5+) and bac7 (10–35) • stachyose (4+), respectively, based on the backbone position cleaved and whether the fragment extends from the N or C terminus. The graphs for the corresponding apo fragment ions produced from the peptide • stachyose complexes and from the apo peptides are shown in Figure S5 (A and B for complexes, C and D for apo peptides). The holo fragment ion plots (A) and (B) reveal stachyose interaction sites, shown as horizontal red bars, based on the presence of overlapping N- and C-terminal holo fragment ions. The bar graphs in (C) and (D) display the variations in fragmentation as difference plots when comparing UVPD of bac7 (1–35) (5+) to bac7 (1–35) • stachyose (5+) (C) and UVPD of bac7 (10–35) (4+) to bac7 (10–35) • stachyose (4+) (D). Negative values indicate suppression of fragmentation of the peptide • stachyose complexes and positive values indicate enhanced fragmentation of the peptide • stachyose complexes relative to the apo peptides. Suppression of fragmentation correlates with increased secondary structure (more stabilized regions), whereas enhancement of fragmentation corresponds to fewer stabilizing non-covalent interactions. Graphs were made with n = 3 samples. Errors for graphs was shown as ± standard deviation.

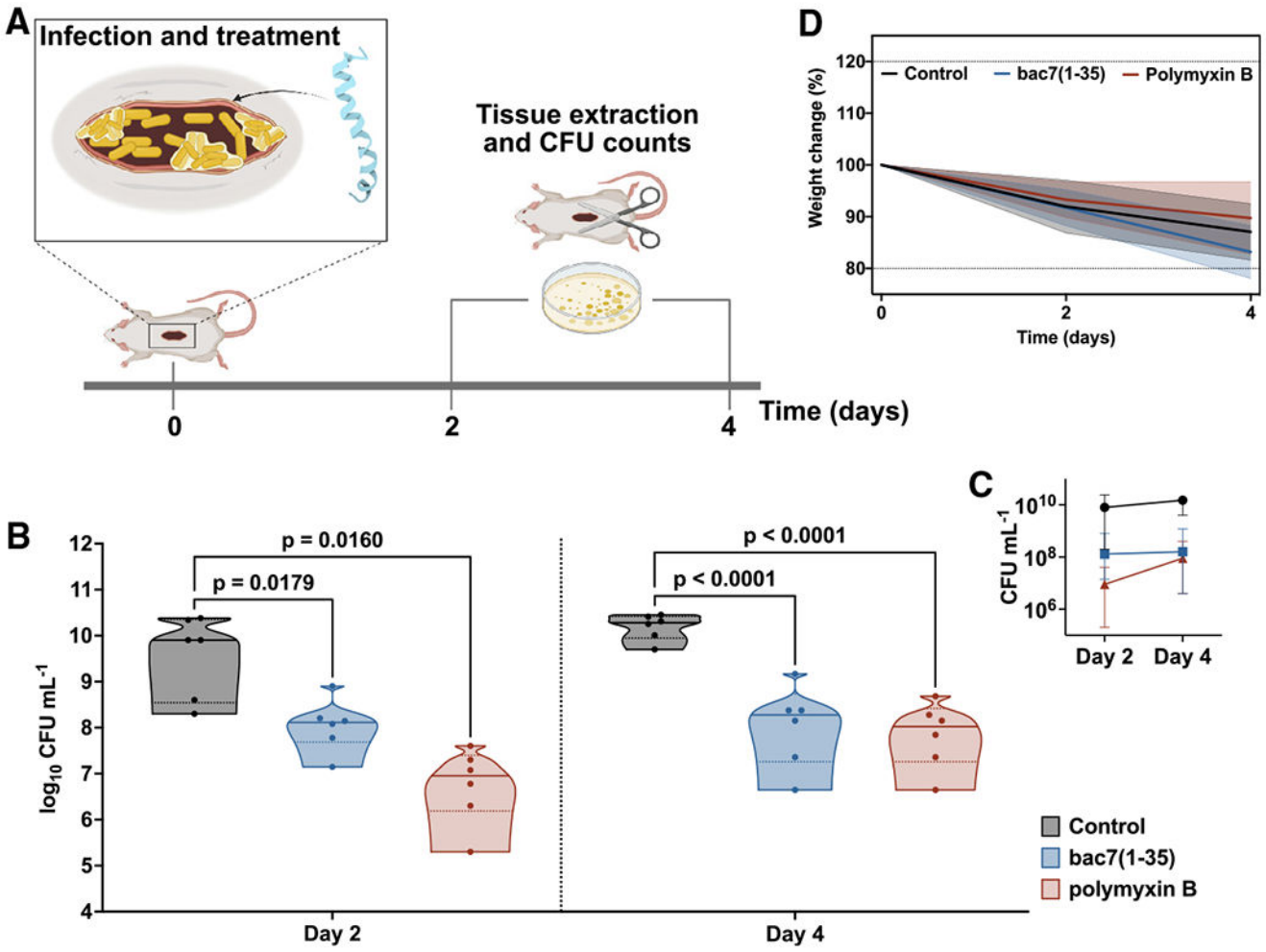

Figure 5. Bac7 (1-35) topical treatment reduces the bacterial burden in a murine skin abscess infection model

Mice had their back shaved and a superficial skin wound was created, a bacterial load of *K. pneumoniae* NTUH K2044 was added onto it, and an abscess was formed (A). One hour after infection, mice were treated with a single dose of bac7 (1–35), polymyxin B positive control, or vehicle only negative controls. Scarified skin areas were excised and quantified at days 2 and 4 (B). The treatments with bac7 (1–35) and polymyxin B caused inhibition of the bacterial growth with up to 2 to 3 orders of magnitude lower bacterial counts over the whole experiment (C). Mouse weight changes, a proxy measure of toxicity, were monitored from the time of the bacterial injection (D). No variations in weight, damage to the skin tissue, or other harmful consequences induced by the bac7 (1–35) or polymyxin B were observed in the mice throughout the experiments. These data are graphed as violin plots to show the median as well as the upper and lower quartiles. Significance was determined using one-way ANOVA followed by Dunnett's test, n = 6 for each group, and p values were obtained by comparing the treated groups to the untreated control group.

Table 1.

Bac7 (1–35) analogs antimicrobial activity toward *K. pneumoniae* NTUH K2044 and aggregation potential with NTUH K2044 extracted polysaccharides

Name	Sequence	#AA	Net charge	MIC[a]	EPSRA[b]
Bac7 (1–35)	RRIRPRPPRLPRPRPRPLPFPRPGPRPIPRPLPFP	35	+11	0.5	1.00
Bac7 (5–35)	PRPPRLPRPRPRPLPFPRPGPRPIPRPLPFP	30	+8	4	0.22
Bac7 (10–35)	LPRPRPRPLPFPRPGPRPIPRPLPFP	26	+6	>42	0.33
Bac7 (1–24)	RRIRPRPPRLPRPRPRPLPFPRPG	24	+9	0.7	0.23
Bac7 (5–24)	PRPPRLPRPRPRPLPFPRPG	20	+6	14	0.16
Bac7 (9–24)	RLPRPRPRPLPFPRPG	16	+5	>67	0.17
Bac7 (1–16)	RRIRPRPPRLPRPRPR	16	+8	1	0.68
Bac7 (1–15)	RRIRPRPPRLPRPRP	15	+7	2	0.19
Bac7 (1–14)	RRIRPRPPRLPRPR	14	+7	2	0.12
Bac7 (1–13)	RRIRPRPPRLPRP	13	+6	>77	0.20
Bac7 (24–59)	PRPIPRPLPFPRPGPRPIPRPLPFPRPGPRPIPRP	35	+8	>32	0.32

#AA, number of amino acids; MIC, minimal inhibitory concentrations; EPS^{RA}, relative extracellular polysaccharide aggregation.

[a] MICs are reported as μmol L^{-1}.

[b] EPS^{RA} is the extracellular polysaccharide aggregation abilities compared with the parental bac7 (1–35) aggregation. Triplicate raw band density numbers used for this comparison are graphed in Figure 3A.